MDPI

Article

Investigations of Hydraulic Power Take-Off Unit Parameters Effects on the Performance of the WAB-WECs in the Different Irregular Sea States

Mohd Afifi Jusoh, Zulkifli Mohd Yusop, Aliashim Albani, Muhamad Zalani Daud [ID] and Mohd Zamri Ibrahim *[ID]

Renewable Energy & Power Research Interest Group (REPRIG), Eastern Corridor Renewable Energy Special Interest Group, Faculty of Ocean Engineering Technology and Informatics, Universiti Malaysia Terengganu, Kuala Nerus 21030, Terengganu, Malaysia; mohd.afifi.jusoh@gmail.com (M.A.J.); zul_12521@yahoo.com (Z.M.Y.); a.albani@umt.edu.my (A.A.); zalani@umt.edu.my (M.Z.D.)
* Correspondence: zam@umt.edu.my; Tel.: +60-96683328

Abstract: Hydraulic power take-off (HPTO) is considered to be one of the most effective power take-off schemes for wave energy conversion systems (WECs). The HPTO unit can be constructed using standard hydraulic components that are readily available from the hydraulic industry market. However, the construction and operation of the HPTO unit are more complex rather than other types of power take-off, as many components parameters need to be considered during the optimization. Generator damping, hydraulic motor displacement, hydraulic cylinder and accumulator size are among the important parameters that influence the HPTO performance in generating usable electricity. Therefore, the influence of these parameters on the amount of generated electrical power from the HPTO unit was investigated in the present study. A simulation study was conducted using MATLAB/Simulink software, in which a complete model of WECs was developed using the Simscape fluids toolbox. During the simulation, each parameters study of the HPTO unit were separately manipulated to investigate its effects on the WECs performance in five different sea states. Finally, the simulated result of the effect of HPTO parameters on the amount of generated electrical power from the HPTO unit in different sea states is given and discussed.

Keywords: ocean wave energy; wave-activated-body; hydraulic power take-off

1. Introduction

Ocean waves are considered as one large untapped and predictable renewable energy resource on earth. Ocean waves contain tremendous of usable energy and have the potential to contribute to a significant share of global renewable energy sources. Ocean wave energy has many advantages such as high energy density, high source availability, source predictability and low environmental impact compared to other renewable energy (RE) sources [1]. The energy density of ocean waves is the highest among all renewable energy sources, which is around 50–100 kW/m [2]. Approximately, 8000–80,000 TWh/year ocean wave energy is available globally [2]. Due to its advantages, electrical energy production from the ocean waves has received a great deal of attention over the past several decades. Numerous wave energy converter systems (WECs) with different harnessing methods have been invented to convert the kinetic energy contained in the ocean waves into usable electricity, as reported in [3–6]. The existing WECs can be classified into wave-activated-body (WAB), oscillating water column (OWC) and overtopping device based on their working principles.

The WAB wave energy converters (WAB-WECs) are also known as oscillating bodies wave energy converters and point absorber wave energy converters. WAB-WECs can be defined as a single body or multiple bodies devices being oscillated by the wave excitation force [7]. WAB-WECs covers a kinds of WEC and recent development of WAB-WECs

around the world has been reported in [4,6,8,9]. In general, these WAB-WECs consist of three main subsystems, namely wave energy converter (WEC), power take-off (PTO) unit, and control system (CS) unit. WEC is a front-end device that absorbs the kinetic energy from the ocean waves. The absorbed energy is then converted to electricity through the PTO unit, whereas the control system unit is used to optimize the electrical energy produced from the WECs during its operation.

PTO is one of the most essential subsystems of WAB-WECs. In recent decades, a wide variety of PTOs have been designed, developed and experimentally tested for numerous types of WEC device, as reported in [10]. The various kinds of PTO concepts can be classified based on their main working principles, such as mechanical–hydraulic, direct mechanical, direct electrical drive, air and hydro turbine. The hydraulic power take-off (HPTO) unit is one of the most reliable and effective PTOs for the WECs [11,12]. The HPTO unit has excellent characteristics, such as high efficiency, wide controllability, well-suited to the low-frequency and large power density of ocean waves, etc. The HPTO unit can also be assembled using standard hydraulic components that are readily available from the hydraulic equipment suppliers. In [11], a review of the most popular HPTO concepts used in WAB-WECs is reported. From the study, the HPTO concepts can be classified into two main groups, i.e., a variable-pressure and a constant-pressure concept. The constant-pressure concept has received more attention. Based on the report in [13], the efficiency of the constant-pressure concept is much higher than that of the variable-pressure concept, which can reach up to 90%. According to [14], several crucial parameters may influence the efficiency of the HPTO unit, such as the mounting position and piston size of the hydraulic actuator, volume capacity and pre-charge pressure of the accumulator, displacement of hydraulic motor and damping coefficient of the electric generator.

Recently, several kinds of research into the HPTO in WAB-WECs have been published for various objectives, for example in [15–21]. From the literature, most of the studies have concentrated on the performance of the HPTO unit without investigating the influence of the important parameters of HPTO. Only a few studies have discussed this issue, e.g., [14,16]. In [14], the influence of the HPTO unit parameters on the power capture ability of two-raft-type of WEC was studied. However, the HPTO concept used in [14] is very different from the HPTO concept considered in the present study. The effects of the HPTO unit on the percentage of power reduction were not discussed in this study. Meanwhile, in [16], the sensitivity of the generator damping coefficient on the average generated electrical power was investigated. From the simulation results, the authors concluded that the generator damping coefficient is relatively sensitive to the changes in wave height and period. However, the sensitivity of the other HPTO parameters was not discussed in [16]. Since there is a lack of published articles on this issue, the present study proposes an investigation of the HPTO unit parameters on the performance of the WAB-WECs. The main objective of the study is to investigate the effect of these important parameters on the electrical power generated from the HPTO unit. The findings can be a useful reference to other researchers for improvement of WECs in future.

The remainder of this paper is organized as follows. Section 2 presents the design of the considered WECS and Section 3 describes the simulation study for investigation of the HPTO parameters. Section 4 presents the results and discussion. Finally, the conclusion and future work are discussed in Section 5.

2. Design of WEC with HPTO Unit

The WEC concept based on [20] is considered in the present study. The simplified concept is shown in Figure 1A. The WECs consist of a single floating body (floater) attached to the fixed body via a hinged arm, which is also known as the WEC device. This WEC device design is almost similar to the concepts used in [13,22–24]. The WEC device is unique due to its ability to convert both wave kinetic energy and wave potential by utilizing the pitch motion of the floater and hinged arm, as presented in Figure 1A. In this system, the WEC is connected to the fixed-body directed to the dominant wave direction to optimally

absorb the kinetic energy from the ocean waves. The WEC device is then connected to the HPTO and the CS unit is placed in the HPTO house to convert the mechanical energy from the WEC device into usable electricity.
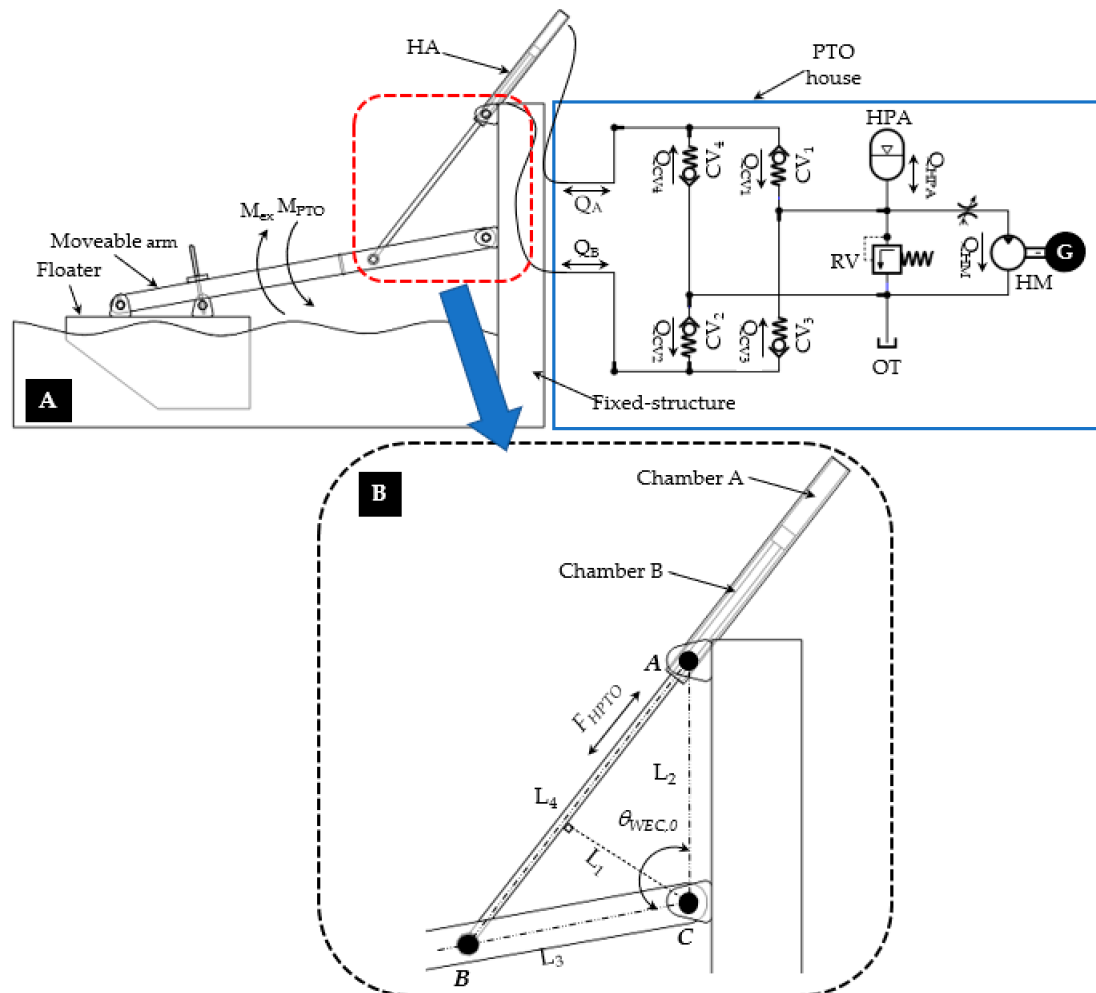

Figure 1. An illustration of WEC with the HPTO unit concept. (**A**) A complete layout design, and (**B**) Enlarge image of the interconnection between HA, floater's arm and fixed structure.

Figure 1A presents the simplified diagram of the HPTO unit which includes a hydraulic actuator (HA), hydraulic hose (HH), check valve rectifier module (CV$_1$, CV$_2$, CV$_3$ & CV$_4$), oil tank (OT), high-pressure and low-pressure accumulators (HPA & LPA), pressure relief valve (RV$_1$ & RV$_2$), hydraulic motor (HM) and electric generator (G). In this concept, double-acting with a single rod type of HA is considered. HA is used as a linear pump to absorb the mechanical energy from the reciprocating motion of the WEC. The piston rod of the HA is attached to the floater's arm using a rod end clevis while the barrel of the HA is attached to the fix-structure. Then, the HA is connected to the check valve rectifier module, an arrangement of four check valves in a bridge circuit configuration, as shown in Figure 1A. The check valve rectifier used in this HPTO unit is similar to the Graetz bridge concept, which is used for conversion of an alternating-current (AC) input into a direct-current (DC) output. For the HPTO, the check valve rectifier module is used to control the fluid flow direction (Q_A & Q_B) from the HA to the HM. Thus, the large chamber (chamber A) of the HA barrel is connected to the inlet and outlet of CV$_1$ and CV$_4$, while the small chamber (chamber B) of the HA barrel is terminated to the inlet and outlet of CV$_2$ and CV$_3$, respectively. The check valve rectifier module is then connected to the HPA and LPA. The HPA is included in the HPTO unit to constrain the pressure of the HM in

the desired ranges. Finally, the generation module which consists of fixed-displacement of HM coupled to G is placed between the HPA and OT. In addition, the pressure relief valves RV_1 & RV_2 are placed to prevent the HPTO unit from over-pressurized fluid flows.

During the operation of WECs, the passing of ocean waves causes a WEC device to pitch upward and downward simultaneously. Then, the reciprocating motion of the WEC device causes back-and-forth motions of the piston and directly generates the high-pressure fluid flow from the HA chambers. During the upward movement of the WEC device, the high-pressure fluid flows from chamber A to chamber B through CV_1, HPA, HM, LPA, and CV_2. On the other hand, during the downward movement, the high-pressure fluid flows from chamber B to chamber A through the CV_3, HPA, HM, LPA, and CV_4 of the WEC device. The high-pressure fluid flowing through the HM causes the HM and G to rotate simultaneously in one direction and thus produces usable electricity. Overall, the speed and torque of the HM depend highly on the characteristics of ocean wave motions such as speed, frequency, wavelength, and amplitude [25]. They also depend on the important parameters of the HPTO unit itself.

2.1. Formulation of Hydrodynamic Pitch Motion of WEC

The hydrodynamic pitch motion of WEC in real waves can be formulated in the time domain to account for the non-linear effects such as the hydrodynamics of a floater, HPTO force, etc. So, the equation for the pitch motion of the WEC device can be expressed by:

$$M_D = M_{ex} - M_{rad} - M_{res} - M_{HPTO} \tag{1}$$

where M_D is the D'Alembert moment of inertia, and M_{ex}, and M_{rad} are the moments due to the diffracted and radiated ocean waves. M_{res} and M_{HPTO} are the moments due to hydrostatic restoring and HPTO unit interactions, respectively. The hydrodynamic pitch motion of the WEC equation above can be extended as follows:

$$(J_{WEC} + J_{add,\infty})\alpha_{WEC}(t) + \int_0^t k_{rad}(t-\tau)\ \omega_{WEC}(t) + k_{res}\ \theta_{WEC}(t) + M_{HPTO}(t) = \int_{-\infty}^{\infty} h_{ex}(t-\tau)\eta_W(\tau)d\tau \tag{2}$$

where J_{WEC} is the moment of inertia of WEC (includes floater and hinged arm), $J_{add,\infty}$ is the added mass at the infinite frequency. τ is the time delay. θ_{WEC}, ω_{WEC} and α_{WEC} are the angular position, angular velocity and angular acceleration of WEC during the pitch motion, respectively. $\theta_{WEC} = 0$ corresponds to the WEC device at rest. k_{rad} and k_{res} are the radiation impulse response function and the hydrostatic restoring coefficients. h_{ex} is the excitation force coefficient and η_W is the undisturbed wave elevation at the center point of the floater. The coefficients of k_{rad}, k_{res} and h_{ex} can be determined from the dynamic diffraction analysis using computational fluid dynamics (CFD) software, such as ANSYS/AQWA, as previously implemented in [20,26–30]. Alternatively, these coefficients also can be obtained using the boundary element method (BEM) toolbox in WAMIT software, as suggested in several studies [31–35].

Since the non-linear effect of the HPTO unit is considered in Equation (2), the moment due to the HPTO unit M_{HPTO} can be described using Equation (3). According to Figure 1B, F_{HPTO} is the feedback force of the PTO unit applied to the WEC device. L_1 is the perpendicular distance between HA and point C, which can be obtained using Equation (4), where L_2 and L_3 are the distance between points *A-C* and *B-C*, respectively. $L_{4,0}$ is the initial distance between points *A-B*. $\theta_{WEC,0}$ and θ_{WEC} are the initial and instantaneous angle of the WEC device. x_p is the linear displacement of the piston. Based on Equation (4), L_1 is always relatively changes according to the change of the arm angle, as illustrated in Figure 1B.

$$M_{HPTO} = F_{HPTO}L_1 \tag{3}$$

$$L_1 = \frac{L_2 L_3 \sin(\theta_{WEC,0} - \theta_{WEC})}{L_{4,0} + x_{HA}} \tag{4}$$

$$x_p = L_{4,0} - \sqrt{L_2^2 + L_3^2 - 2L_2L_3\cos(\theta_{WEC,0} - \theta_{WEC})} \tag{5}$$

2.2. Formulation of HPTO Unit

Technically, the force generated by the HPTO unit, F_{HPTO} is represented by the feedback force applied by the HA to the WEC device. The nonlinear F_{HPTO} is generated due to the dynamic pressure in chambers A and B (P_A & P_B) and the piston friction force (F_{fric}) of the HA. The F_{HPTO} can be expressed using Equation (6), where $A_{p,A}$ and $A_{p,B}$ are the sectional areas of the piston in chambers A and B, respectively. $A_{p,A}$ and $A_{p,B}$ can be obtained using Equations (7) and (8), where d_p and d_r are the piston and rod diameter of the HA. Meanwhile, the dynamics of P_A and P_B can be calculated according to the fluid continuity function, as described in Equations (9) and (10), where β_{eff} is the bulk modulus of the hydraulic fluid. Q_{CV1} to Q_{CV4} are the flow rates across the check valves CV_1 to CV_4. L_s, x_p and $\dot{x}_p$ are the stroke length, linear displacement and linear velocity of the piston, respectively.

$$F_{HPTO} = P_A A_{p,A} - P_B A_{p,B} + F_{fric} \tag{6}$$

$$A_{p,A} = \pi d_p^2/4 \tag{7}$$

$$A_{p,B} = \pi\left(d_p^2 - d_r^2\right)/4 \tag{8}$$

$$\frac{d}{dt}P_A = \frac{\beta_{eff}}{A_{p,A}(L_s - x_p)}\left(\dot{x}_p A_{p,A} + Q_{CV4} - Q_{CV1}\right) \tag{9}$$

$$\frac{d}{dt}P_B = \frac{\beta_{eff}}{A_{p,B}(L_s - x_p)}\left(\dot{x}_p A_{p,B} + Q_{CV2} - Q_{CV3}\right) \tag{10}$$

The flow rates Q_{CV1} to Q_{CV4} can be generally calculated using Equation (11), where C_d and A_{CV} are the discharge coefficient and the working area of each check valve. P_{CVin} and P_{CVout} are the inlet and outlet pressure of each check valve. ρ_{oil} is the hydraulic oil density.

$$Q_{CV} = \begin{cases} C_d A_{CV}\sqrt{\frac{2}{\rho_{oil}}|P_{CVin} - P_{CVout}|} & ,if\ P_{CVin} > P_{CVout} \\ 0 & ,if\ P_{CVin} < P_{CVout} \end{cases} \tag{11}$$

On the other hand, the fluid volume (V_{HPA}) and flow rate (Q_{HPA}) which enters the accumulator can be calculated using Equations (12) and (13), where $V_{HPA,cap}$ is a capacity, $P_{HPA,0}$ is the initial pressure and $P_{HPA,in}$ is the inlet gauge pressure of HPA, and n is the specific heat ratio, respectively. The initial pressure in the accumulators depends on the pre-charge pressure of the nitrogen gas in the HPA bladder.

$$V_{HPA} = \begin{cases} V_{HPA,cap}\left[1 - \left(\frac{P_{HPA,0}}{P_{HPA,in}}\right)^{\frac{1}{n}}\right] & ,\ if\ P_{HPA,in} > P_{HPA,0} \\ 0 & ,\ if\ P_{HPA,in} \leq P_{HPA,0} \end{cases} \tag{12}$$

$$Q_{HPA} = \dot{V}_{HPA} = \begin{cases} \frac{1}{n}V_{HPA,cap}\left(1 - \frac{P_{HPA,0}}{P_{HPA,in}}\right)^{\frac{1-n}{n}}\frac{P_{HPA,0}\dot{P}_{HPA,in}}{P_{HPA,in}^2} & ,\ if\ P_{HPA,in} > P_{HPA,0} \\ 0 & ,\ if\ P_{HPA,in} \leq P_{HPA,0} \end{cases} \tag{13}$$

Meanwhile, the flow rate across the HM (Q_{HM}) and the actual torque of HM (τ_{HM}) can be obtained using Equations (14) and (15), where D_{HM}, ω_{HM} and ΔP_{HM} are the displacement, angular speed and the internal pressure difference of HM. $\eta_{HM,V}$ and $\eta_{HM,M}$ are the volumetric and mechanical efficiency of HM.

$$Q_{HM} = D_{HM}\omega_{HM}/\eta_{HM,V} \tag{14}$$

$$\tau_{HM} = \Delta P_{HM}D_{HM}\eta_{HM,M}/2\pi \tag{15}$$

Finally, the electric power generated by the electric generator (P_G) can be expressed using Equation (16), where ω_G, τ_G and η_G are angular speed, the torque and overall efficiency of the electrical generator. Since the electrical generator and HM are rotating simultaneously, the ω_G and τ_G are equal to ω_{HM} and τ_{HM}, respectively.

$$P_G = 2\pi\omega_G\tau_G\eta_G = 2\pi\omega_{HM}\tau_{HM}\eta_G \tag{16}$$

2.3. Main Parameters of HPTO Unit

As previously mentioned in [14], there are several important parameters affecting the performance of the HPTO unit such as piston diameter, the volume capacity of HPA, displacement of HM, etc. Table 1 provides the important parameters of the HPTO unit that are summarized from Equations (3)–(16). For some parameters, the higher and lower values can reduce the performance of the HPTO unit. To investigate this problem, a detailed study regarding the influence of these parameters on the overall performance of WECs is performed in the present study.

Table 1. Important parameters of the HPTO unit.

No.	Important Parameters of HPTO	Unit
1	Vertical mounting of HA, L_2	m
2	Piston diameter, d_p	m
3	Volume capacity of HPA, $V_{HPA,cap}$	L
4	Pre − charge gas pressure of HPA, $P_{HPA,0}$	bar
5	Displacement of HM, D_{HM}	cc/rev
6	Damping coefficient of the generator, d_G	Nm/(rad/s)

In the present study, the complete simulation investigation of HPTO unit parameters was implemented in the MATLAB/Simulink software (Version: 2018b). The detailed methodology of the present study is described in the following subsections.

3. Simulation Investigation of HPTO Unit Parameters

3.1. Simulation Set-up of WEC with HPTO Unit

The MATLAB/Simulink software was used in this study to model a complete WEC system shown in Figure 1. The WECs consists of two main parts, the WEC model and the HPTO model. The WEC model was developed using a mathematical function block based on Equations (1)–(5). The wave elevation data, η_W and F_{HPTO} are the inputs, while the x_p is the output of the WEC model. According to Equations (1) and (2), the hydrodynamics parameters of the WEC device such as k_{rad}, k_{res}, h_{ex}, added mass coefficient (k_{add}) and impulse response function (k_{imp}) are required to develop the considered WEC model. The hydrodynamic parameters of the WEC model from the previous study in [20] were used, since a similar WEC concept was considered in this study. In [20], these hydrodynamic parameters were obtained from the frequency domain analysis study that was carried out using ANSYS/AQWA software. The obtained hydrodynamic parameters are presented in Figure 2.
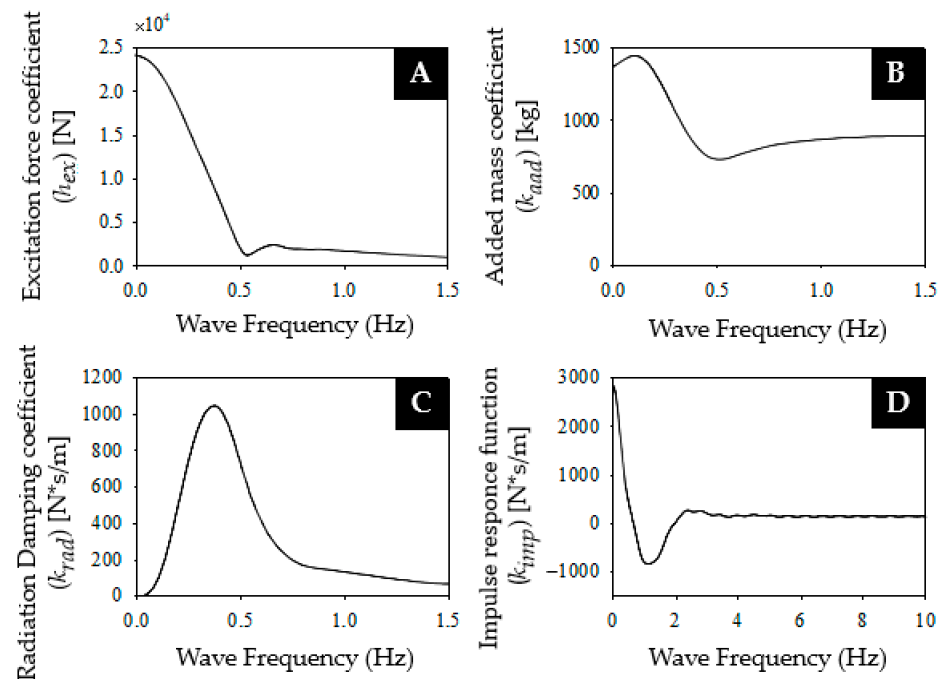
Figure 2. Hydrodynamic parameters of WEC device. (**A**) Excitation force coefficient, (**B**) Added mass coefficient, (**C**) Radiation damping coefficient, and (**D**) Impulse response function.

Meanwhile, the Simscape SimHydraulic toolbox in MATLAB/Simulink was used to develop the HPTO unit model. The snapshot of the developed model in MATLAB/Simulink is depicted in Figure 3. As illustrated in the figure, x_p is the input of the HPTO unit. Using x_p signal, the linear velocity of the piston, $\dot{x}_p$ is obtained using a first-order lag-based linear displacement to linear velocity converter. The double-acting hydraulic cylinder (DAC) component was used as HA. In the Simscape SimHydraulic toolbox, the DAC component is constructed based on the translational hydro-mechanical converter and translational hard stop blocks. The rod motion is limited with the mechanical translational hard stop block. The ideal force sensor block was connected to the HA rod to measure the F_{HPTO}. The pressure and flow rate sensor blocks were also connected to the HA to measure the dynamic pressure and flow rate of HA. To account for the friction loss along the pipe length and the fluid compressibility, the hydraulic pipeline blocks were used to connect some of the components, as illustrated in Figure 3. The thermodynamic transformation in the HPA was assumed to be isentropic, which is reasonable considering the cycle time in the device. Furthermore, for ease of control, a simple rotational damper with varying damping coefficients was used to represent the electric generator unit. In this way, the resistive torque imposed by the electric generator can be manipulated by varying the value of the damping coefficient (d_G). The generated electric power from the electric generator can be calculated using Equation (16). In this study, the initial parameters of the HPTO unit were manual tuned. However, these parameters are not optimal yet. The detailed specifications of each component in the developed HPTO model are provided in Table 2. Finally, the developed HPTO unit model in MATLAB/Simulink was then experimentally validated using an actual HPTO test rig in the dry lab environment.
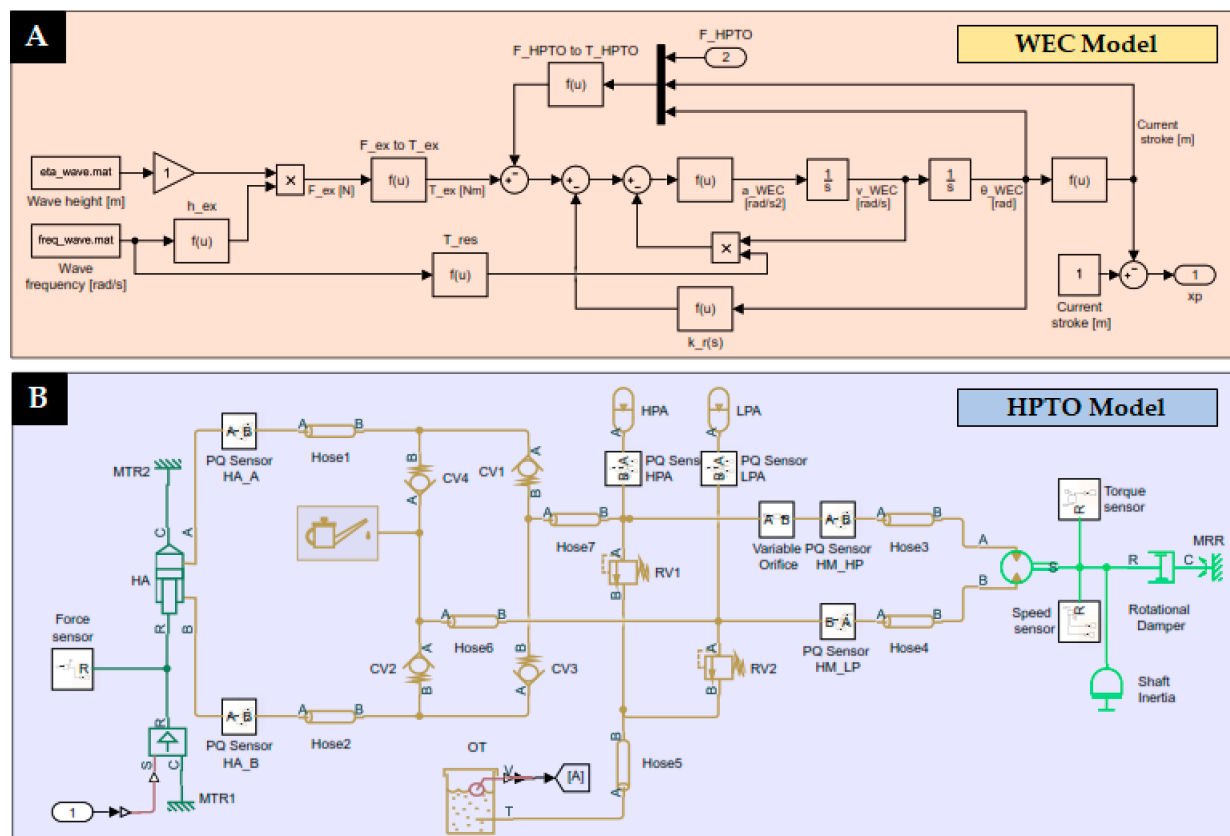
Figure 3. A complete model of WEC with HPTO unit in MATLAB/Simulink. (**A**) WEC device model, and (**B**) HPTO unit model.

Table 2. Detailed specifications of the developed HPTO unit.

Component Descriptions		Value	Unit
Hydraulic actuator	Piston diameter, d_p	0.035	m
	Piston rod diameter, d_r	0.022	m
	Stroke length, L_s	0.3	m
	Initial stroke length, $L_{s,0}$	0.15	m
	Vertical distance mounting, L_2	0.5	m
	Horizontal distance mounting, L_3	0.5	m
	Initial rod length (point A to B), L_4	0.766	m
High-pressure accumulator	Pre-charge pressure, $P_{HPA,0}$	46.9	bar
	Volume capacity, $V_{HPA,cap}$	2.8	L
	Adiabatic index, γ	1.4	-
Low-pressure accumulator	Pre-charge pressure, $P_{LPA,0}$	3.2	bar
	Volume capacity, $V_{LPA,cap}$	4.0	L
	Adiabatic index, γ	1.4	-
Hydraulic motor	Displacement, D_{HM}	8.4	cc/rev
	Nominal shaft angular velocity, $\omega_{HM, nom}$	200	rpm
	Volumetric efficiency at nominal condition, $\eta_{HM, V}$	0.92	-
	No-load torque, $\tau_{HM, no}$	0.05	Nm
Electric generator	Rated power, $P_{G, rated}$	100	W
	Rated speed, $\omega_{G, rated}$	200	rpm
	Rated torque, $\tau_{G, rated}$	6.0	Nm
	Damping coefficient, d_G	0.03	Nm/(rad/s)
	Moment of inertia	0.0036	kg/m^2
Fluid properties	Density, D_{oil}	50	kg/m^3
	Viscosity, Vis_{oil}	850	cSt

3.2. Simulation of WEC with HPTO Unit Using Five Irregular Sea States

The simulation analysis was started with the performance evaluation of the WEC with the HPTO model, using five different irregular wave input conditions. This simulation was intended to evaluate the effect of the significant wave height (H_W) and the peak wave period T_W on the electrical output power produced by the HPTO unit. Five different sea states were considered as summarized in Table 3. Sea state A is the nominal wave condition for the developed WEC with the HPTO model, in which the significant wave height and the peak wave period were set to 0.8 m and 2.5 s, respectively. Sea state B and C were considered for wave height case studies, while sea state D and E are for wave period case studies. For sea states B and C, the significant wave heights were set to 0.6 m and 1.0 m, which is ±0.2 m of the wave height in sea state A. Meanwhile, the peak wave periods for both states were maintained at the nominal value. For sea states D and E, the significant wave height was maintained at the nominal value, while the peak wave periods were set to 2.0 s and 3.0 s, which is ±0.5 s of the nominal wave period.

Table 3. The parameters of five different sea states.

Sea State	Significant		Remarks
	Wave Height, H_W (m)	Wave Period, T_W (s)	
A	0.8	2.5	Nominal wave condition
B	0.6	2.5	Wave height case
C	1.0		
D	0.8	2.0	Wave period case
E		3.0	

3.3. Investigation Studies of HPTO Unit Parameters

A further simulation proceeded with the investigation of the HPTO unit parameters study. As previously mentioned, the main purpose of the study is to investigate the influence of the important parameters on the performance of the HPTO unit. Thus, from this study, how the performance of the HPTO unit varies to its configuration parameters was discovered. To achieve the objective, several case studies were conducted on the developed simulation model of WECs. A summary of the case studies is provided in Table 4. The regulating condition of each case was selected based on the availability of the components from the hydraulic equipment market.

Table 4. Detailed of the case studies.

Case	Important Parameters of HPTO	Default Value	Regulating Condition		Unit
			Ranges	Step	
1	Vertical Mounting of HA, L_2	0.5	0.1–0.7	0.1	m
2	Piston diameter, d_p	0.035	0.025–0.060	0.005	m
3	Volume capacity of HPA, $V_{HPA,cap}$	2.8	0.5–10.5	2.0	L
4	Pre-charge gas pressure of HPA, $P_{HPA,0}$	46.9	20–80	10.0	bar
5	Displacement of HM, D_{HM}	8.4	6–18	2	cc/rev
6	Damping coefficient of the generator, d_G	0.287	0.1–1.3	0.2	Nm/(rad/s)

4. Results and Discussion

The results from the investigation simulations are presented and discussed in three sections. The first Section 4.1 presents the experimental validation of the developed WEC with the HPTO unit model. The second Section 4.2 provides the performance analysis of the developed WEC with the HPTO unit model in different sea states and the third Section 4.3 presents the finding from the investigations of the influence parameters on the HPTO unit performance.

4.1. Experimental Validation of the HPTO Model

Figure 4A shows the hardware in the loop (HIL) test rig of the HPTO unit. In general, the HIL test rig was developed based on the design of WECs in Figure 1 and several sensors were installed to monitor the variations of HPTO force, oil pressure, the oil level in the oil tank and as the hydraulic motor shaft speed, as illustrated in Figure 4B. The servo-electric actuator was also installed in the HIL test rig to replicate wave-induced relative pitch motion to drive the HPTO unit to capture the wave energy. A servo motor controller based on Labview/Arduino integration and the data acquisition system for data collection from the sensors were placed in the control system unit. The relative pitch motion generated by the electric actuator is according to the input wave state. To simulate the condition that is close to real-world application, the hydrodynamic parameters from the CFD analysis and the feedback HPTO force were considered to calculate the produced excitation force applied to the floater's arm. The sinusoidal wave input with the amplitude and period of 0.4 m and 2.5 s were considered for the validation of HPTO model. The captured image of maximum upward and downward motions of the HIL test rig during the experimental validation of the HPTO unit is depicted in Figure 4C,D.
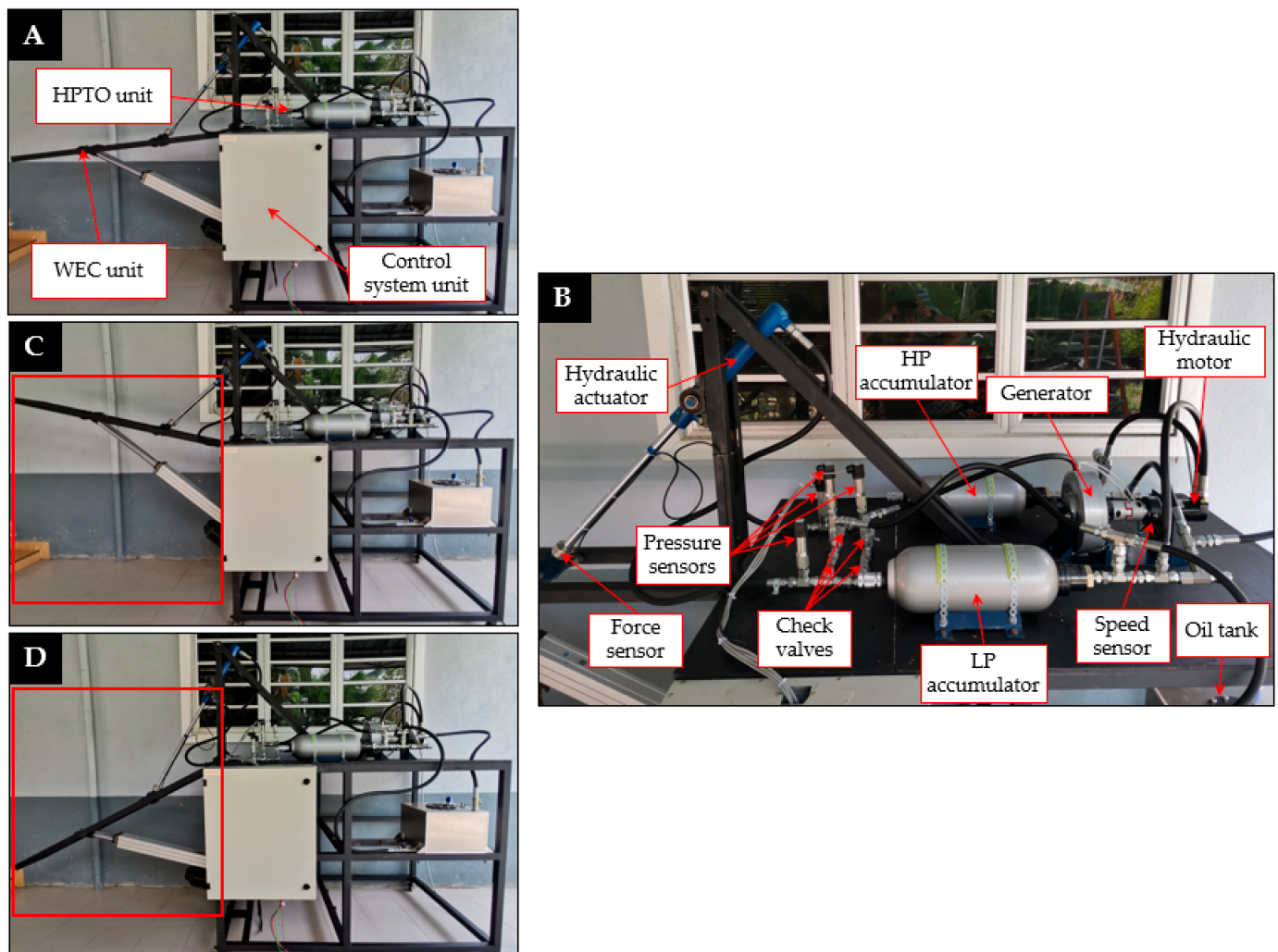

Figure 4. Experimental evaluation of WEC with hydraulic PTO unit. (**A**) A complete dry-lab test rig, (**B**) Enlarge image of HPTO unit setup, (**C**) Maximum upward, and (**D**) Maximum downward position of the WEC device.

Figure 5 shows the results of the behaviour of the HPTO unit in a regular wave condition with an amplitude and period of 0.4 m and 2.5 s. From the figure, it can be seen that the simulation results of the developed WEC with the HPTO unit model in

MATLAB/Simulink is in good agreement with the results obtained from the HIL test rig. However, slight differences and some fluctuations in hydraulic motor speed and HPTO force results were obtained during the experiment, as depicted in Figure 5A,B. These differences and fluctuations may be attributed to the errors in the manufacture and assembly of the test rig, the measuring errors of the transducers, the vibration of the hydraulic motor, and the leakage in the hydraulic motor, cylinders and joints. Such a good agreement presented in Figure 5A,B indicates that the developed WEC with HPTO unit model in MATLAB/Simulink presented in the present study would be effective and reliable as a tool for predicting the amount of power that can be generated from the ocean waves.
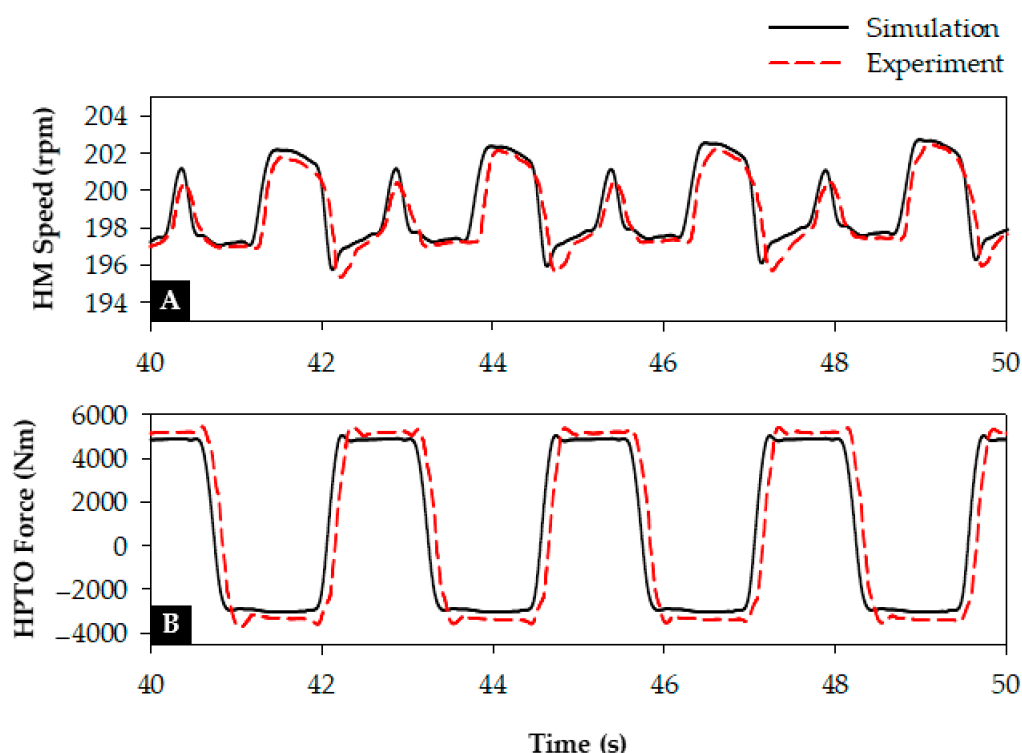

Figure 5. Behaviour of HPTO unit in a regular wave condition. (**A**) Speed of hydraulic motor and (**B**) HPTO force applied to the floater's arm.

4.2. Performance of WEC with HPTO Model in Five Irregular Sea States

The simulations of the developed WEC with the HPTO unit model using different sea states was first carried out in the present study. This simulation was intended to evaluate the performance of the developed model against the different wave heights and periods. The simulation was started with the nominal sea state (sea state A) and the results from the simulation are presented in Figures 6 and 7. Figure 6A shows the responses of WEC and the hydraulic cylinder piston against the irregular wave input in sea state A. The figure shows that the displacement of the WEC device was slightly lower than the wave elevation, particularly during the upward motion. This is due to influencing factors such as the hydrostatic restoring moment, the moment due to the HPTO unit and the initial moments of floater and arm [36]. Based on the results, the average displacement of the WEC device and hydraulic piston was 70% and 15% of the wave elevation. The figure also depicts that the displacements of the WEC device and piston were slightly delayed from the wave elevation. Figure 6B presents the profile of the HPTO force applied to the WEC device. On average, the HPTO forces applied to the WEC device during upward and downward motion equaled 3.64 kN and 1.99 kN, respectively. The unbalanced HPTO force applied to the WEC device is due to the unsymmetrical effective area of the piston. A larger effective area of piston produced a higher force rather than a smaller effective area piston.

Figure 6C shows the profile of HPA pressure. From the figure, the pressure of HPA reached up to 49 bar several times, which was a 4.5% increased from its pre-charge pressure setting.
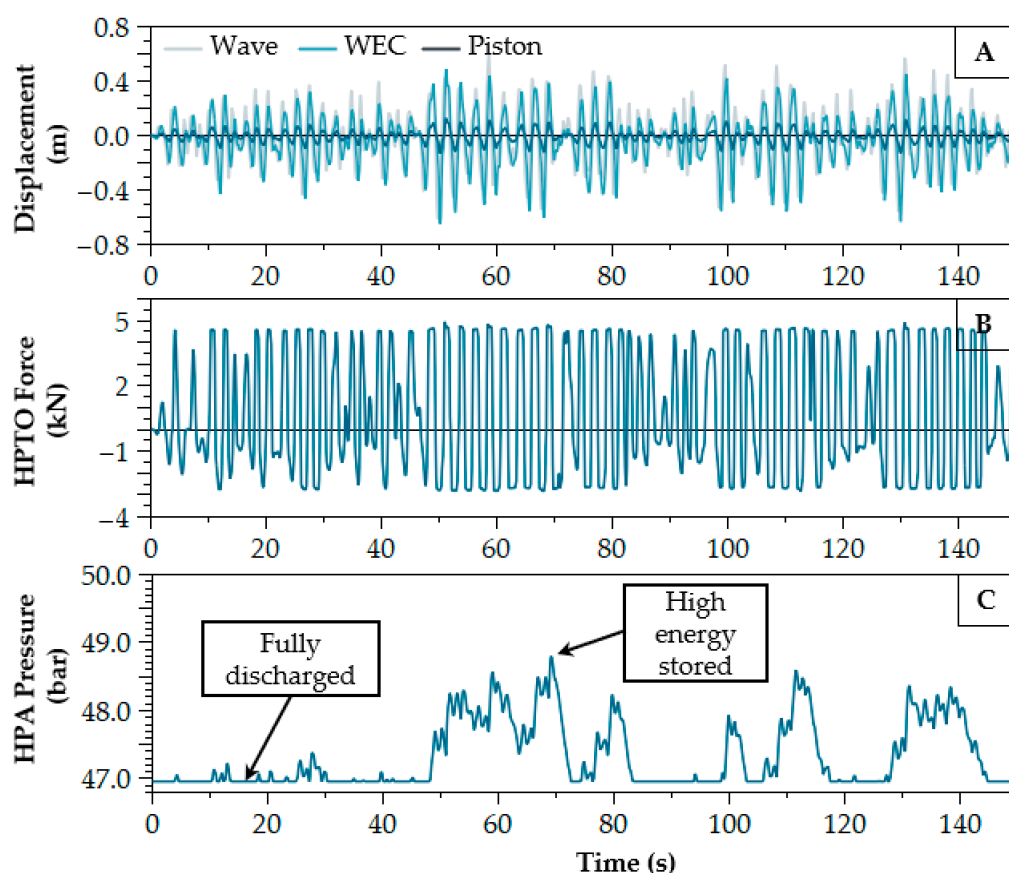

Figure 6. Performance of WEC with HPTO unit in sea state A, (**A**) Displacement of Wave, WEC and hydraulic cylinder piston, (**B**) HPTO force applied to WEC device, and (**C**) Pressure of high-pressure accumulator.

Meanwhile, Figure 7A,B show the pressure and speed profile of the HM. It can be seen from the figures that the pressure and the speed of the hydraulic motor reached up to 49 bar and 200 rpm. The smoothing effect of the HPA unit on the hydraulic motor pressure can be seen in Figure 7A. The HPA was able to reduce the fluctuation of the hydraulic motor pressure, particularly after 50 s of HPTO operation. Figure 7C illustrates the profile of the generated power from the HPTO unit. The average power generated from the generator was 70.9% of its rated capacity (100 W). The figure also demonstrates that some fluctuations exist in the generated power from the generator, particularly at the early stage of the operation. The comparison simulation results of the WEC with HPTO unit in each sea state are summarized in Table 5. From the table, the simulation result showed that the significant wave height and peak wave period were affected by the overall performance of the WEC with the HPO unit. First, the table reveals that the averaged angular displacement of the WEC device was increased and decreased, relatively, with increases and decreases of the significant wave height and peak wave period. From the table, the angular displacement of the WEC device in sea states B and D were reduced by 38% and 33% (upward) and 24% and 21% (downward) of its angular displacement in the nominal sea state. Meanwhile, the angular displacement in the sea states C and E were increased by 21% and 16% (upward) and 28% and 18% (downward), respectively. The increase and decrease of the angular displacements are due to the increase and decrease HPTO force applied to the WEC device, which can be obtained in Table 5. The increase and decrease of WEC displacement, relatively, also increase and decrease the generated

output power from the HPTO unit. As can be seen, the average power generated from the HPTO unit in sea states B and D were decreased by 41% and 34% of power from sea state A, while 15.5% and 10.4% were increased in sea states C and E. Overall, the generated power from the HPTO unit in each sea state is below its rated capacity. Thus, several parameter optimization methods, as suggested in [20], can be further implemented to increase the generated power from the HPTO unit.
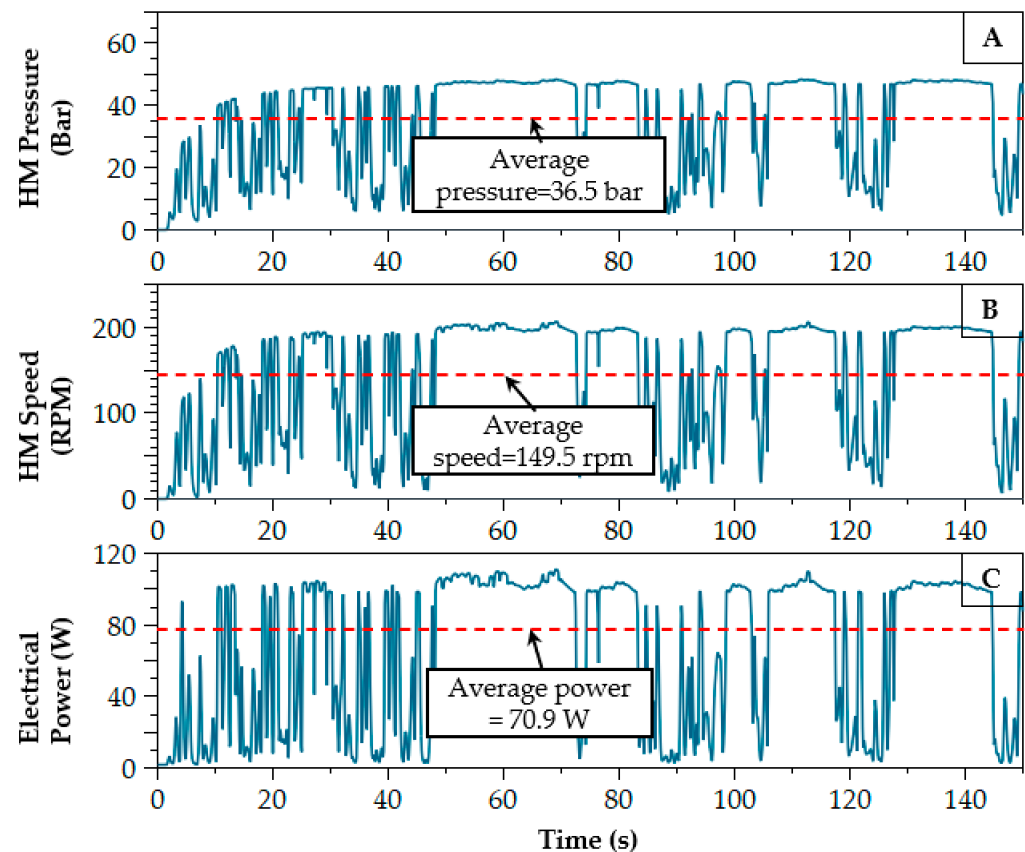

Figure 7. Performance of WEC with HPTO unit in sea state A (continue), (**A**) Pressure of hydraulic motor, (**B**) Speed of hydraulic motor, and (**C**) Electrical power generated from HPTO unit.

Table 5. Performance of WEC with HPTO unit in different sea states.

Performance Description (Unit)		Sea State				
		A	B	C	D	E
Averaged Angular Displacement of WEC (°)	upward	5.73	3.53	6.94	3.84	6.67
	downward	6.95	5.26	8.87	5.49	8.17
Averaged piston displacement (m)	upward	0.033	0.019	0.041	0.022	0.038
	downward	0.035	0.026	0.043	0.028	0.040
Averaged HPTO force (kN)	upward	3.64	3.49	4.45	3.54	4.09
	downward	1.99	1.63	2.42	1.73	2.24
Averaged operating pressure of HM (bar)	-	36.5	27.4	41.9	29.2	39.7
Averaged speed of generator (rpm)	-	149.5	109.1	173.6	117.2	164.4
Averaged generated electrical power (W)	-	70.9	41.7	81.8	47.1	78.2

4.3. Investigation Studies of HPTO Unit Parameters

In this subsection, the influence of each HPTO unit parameter on the generator power in five different sea states is discussed. From this subsection, how the power of the generator varies with the considered HPTO parameters and their corresponding to the sea states can be discovered in the following subsection.

4.3.1. Case 1: Position of Hydraulic Cylinder

The influence of HA position on the power of the generator was firstly investigated in this study. For this case, the position of HA was manipulated by adjusting the L_2 and L_3, as indicated in Figure 1. In this case, L_2 was incrementally varied by 0.1 m within the range of 0.1 to 0.7 m. To be fair, during adjustment of the HA position, the initial rod length of HA from point A to B (L_4) was maintained as default for every sequence. Figure 8 depicts that the averaged power generated from the generator varies with the vertical mounting distance of HA for different sea states. The figure clearly illustrates that the averaged power generated from the generator increases along with the increase of the horizontal mounting of HA for all sea states. Then, it decreases after reaching the optimal mounting position. From the figure, the optimal values for L_2 are different for each sea state. For the small wave height and period sea states (sea states B and D), the optimal value for L_2 is smaller than for the case of large wave height and period sea states. At the optimal mounting position, averaged generated power for the sea states A to E were around 72 W, 42 W, 84 W, 47 W and 79 W, respectively. At the lower L_2, averaged generated power for all sea states were significantly reduced compared to the bigger value of L_2, as depicted in Figure 8. For example, at L_2 equal to 0.1 m, the averaged generated power from the generator for the sea states A to E were reduced by 88%, 91%, 82%, 90% and 84% of their optimal values. While at L_2 equal to 0.7 m, the averaged power generated from the generator for sea states A to E were reduced by 43%, 53%, 32%, 51% and 38% of their optimal values, respectively. The percentage of averaged power reduction also indicates that the mounting position of HA relies on the wave height and wave period. The percentage of averaged power reduction shows that the mounting position of HA was more affected by low height and a small period for the sea states. Technically, the huge reduction of the averaged power generated at the lower L_2 is due to the larger HPTO force applied to the WEC device. So, from these investigation results, it can be suggested that the distance of L_2 should be equal or larger than L_3 to prevent huge losses due to the mounting position of HA.
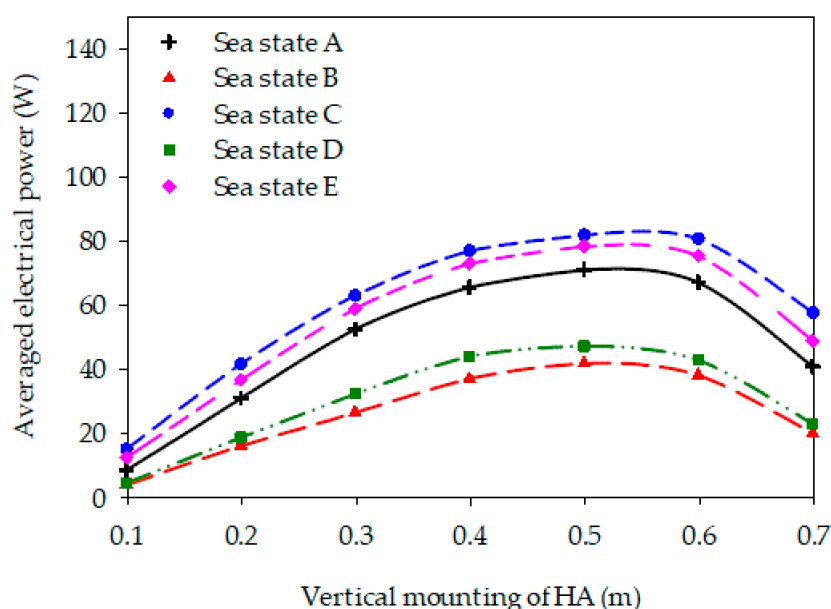

Figure 8. Averaged power of generator versus horizontal mounting distance corresponding to different sea states.

4.3.2. Case 2: Piston Size of the Hydraulic Actuator

The influence of the effective area of the piston in both hydraulic actuator chambers is also a concern in this study. As previously shown in Equation (6), the effective piston area relatively affects the amount of feedback HPTO force F_{HPTO} applied to the WEC device. From Equations (7) and (8), the effective area of the piston in both hydraulic chambers can

be calculated via the diameter size of piston and rod (d_p and d_r). Since a double-acting with single rod hydraulic actuator was considered in this study, the effective piston area in chamber B is affected by the rod size. This means that the effective piston area in chamber A is larger than that in chamber B. To investigate, the wide range of d_p was used to examine the performance of the HPTO unit. In this case, the values of d_p was incrementally varied by 0.005 m within the range of 0.025 to 0.060 m. In this case, the minimum range was selected based on the smallest piston size that is currently available in the hydraulic equipment market. While the value of d_r remains as the initial parameter setting. Figure 9 presents the effect of the piston and rod diameter on the averaged power generated from the generator in different sea states. From the figure, it can be observed that the averaged generated power is influenced by the piston size of the hydraulic actuator. The figure depicts that the averaged generated power first increases with the increase of the piston diameter size and then starts to decrease after obtaining the optimal value of d_p. From the figure, it is clearly shown that the smaller significant wave height and peak period sea states were more affected by the piston size. The result shows that the average generated power for sea states B and D started to decrease after 0.045 m size of the piston, while for the bigger wave height and period sea states, such as sea state A, C and E, the average generated power started to decrease after 0.050 m and 0.055 m, respectively. This may be due to the lower wave forces during sea states B and D compared to wave forces for sea states A, C and E. Technically, more high-pressured fluid can be supplied to the hydraulic motor by a hydraulic actuator with a larger piston size. As a result, the average generated power at the optimal point for sea states A, C and E were found to be 94 W, 118 W and 110 W. Meanwhile, the average generated power at the optimal point for sea states B and D were found to be 64 W and 70 W, respectively.
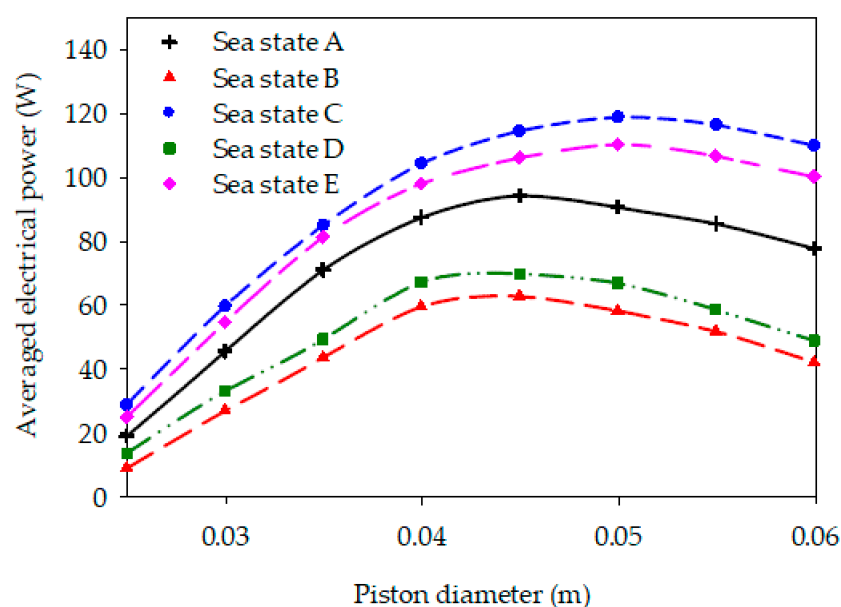

Figure 9. Averaged power of generator versus piston diameter corresponding to different sea states.

4.3.3. Case 3: Volume Capacity of HPA

The accumulator plays an important role in mitigating the power fluctuation during a dynamic process of wave power conversion. By using HPA and a robust control strategy, the HPTO unit enables conversion of the high fluctuating wave power into a smooth and continuous electrical power. Since the HPA is more important to the HPTO unit, a further investigation into the main parameters of HPA, such as volume capacity ($V_{HPA,cap}$) should be conducted. Hence, the effect of the volume capacity of HPA on the HPTO performance was explored in the present study. A wide range of $V_{HPA,cap}$ was used to evaluate its effect on the averaged generator power corresponding to the different sea states. In this

case, the value of $V_{HPA,cap}$ was incrementally varied by 2 L within the range of 0.5 to 10.5 L, as previously mentioned in Table 4. Figure 10 presents the effect of $V_{HPA,cap}$ on the averaged generated power from the generator for the different sea states. The figure showed that the averaged power generated from the generator is influenced by the increase of $V_{HPA,cap}$, particularly for large significant wave height and peak period sea states, while there was a less significant effect for small significant wave height and peak period sea states. From the result, the average generated power, particularly for sea states C and E significantly reduced by the increase of $V_{HPA,cap}$. By changing the value of $V_{HPA,cap}$ from 0.5 L to 10.5 L, the average generated power for sea states C and E were reduced by 28% and 20%, respectively. This power reduction can be attributed to more energy accumulated in the HPA, rather than directly flowing to the hydraulic motor when the large capacity of the HPA is implemented.
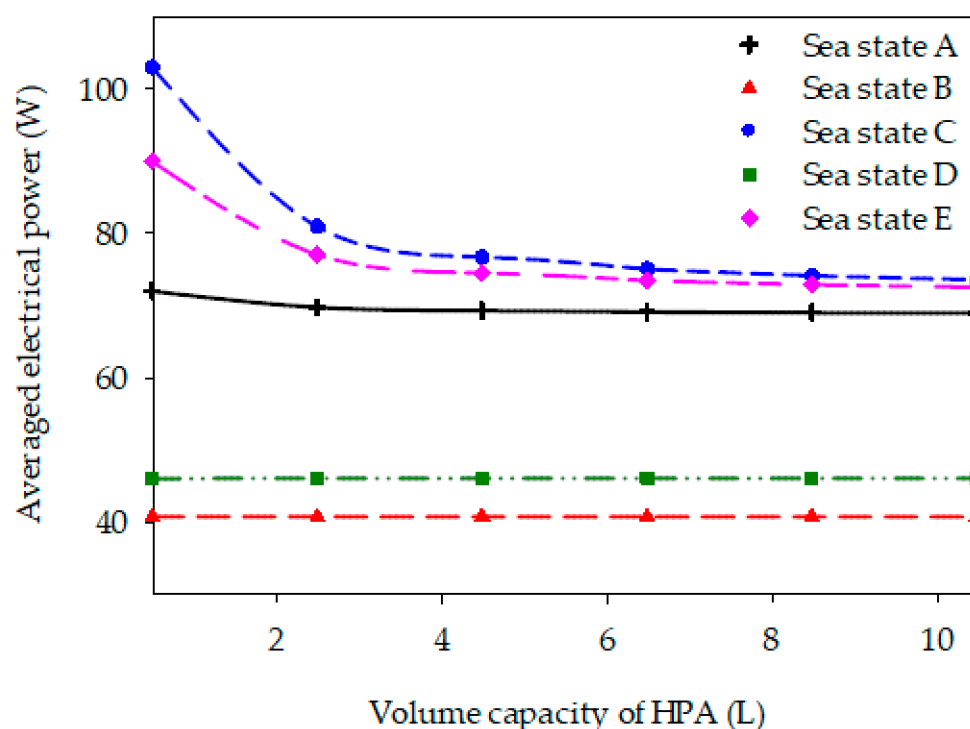

Figure 10. Averaged power of generator versus volume capacity of HPA corresponding to different sea states.

4.3.4. Case 4: Pre-Charge Pressure of HPA

The pre-charge pressure of HPA ($P_{HPA,0}$) is another important parameter of the HPTO. Technically, $P_{HPA,0}$ determines how much hydraulic fluid will remain accumulated in the HPA. The charging process of HPA begins when hydraulic fluid flows into the fluid chamber when the HPTO unit pressure is greater than the $P_{HPA,0}$. During charging, the gas is compressed to store energy. Once the HPTO unit pressure is below $P_{HPA,0}$ level, the high-pressure nitrogen gas in the ballast forces hydraulic fluid from the fluid chamber into the hydraulic motor. For such a dynamic process, the investigation of the effect of the $P_{HPA,0}$ on the power of the generator was considered. In this case, the value of $P_{HPA,0}$ was incrementally increase by 10 bar within the range of 20 to 80 bar. Figure 11 presents the variation of $P_{HPA,0}$ on the averaged generated power from the generator for different sea states. As can be seen in the figure, for all sea states the average power of the generator slightly increased, and then tended to be steady after the $P_{HPA,0}$ reached an optimal of $P_{HPA,0}$. The figure showed that a higher level of $P_{HPA,0}$ can be used for large significant wave height and peak period sea states. For example, the level of $P_{HPA,0}$ can be set up to 70 bar for sea states C and E, while, the highest $P_{HPA,0}$ for sea states, B and D was only

up to 40 bar. This difference is due to the different operating pressure of HPTO in each sea state, in which the operating pressure of HPTO is higher in sea states C and E rather than sea state B and D. The averaged generated power at the optimal point for sea state A, C and E were reached up to 80 W, 124 W and 108 W, while for sea states B and D the averaged generated power at the optimal point only reached 43 W and 49 W, respectively.
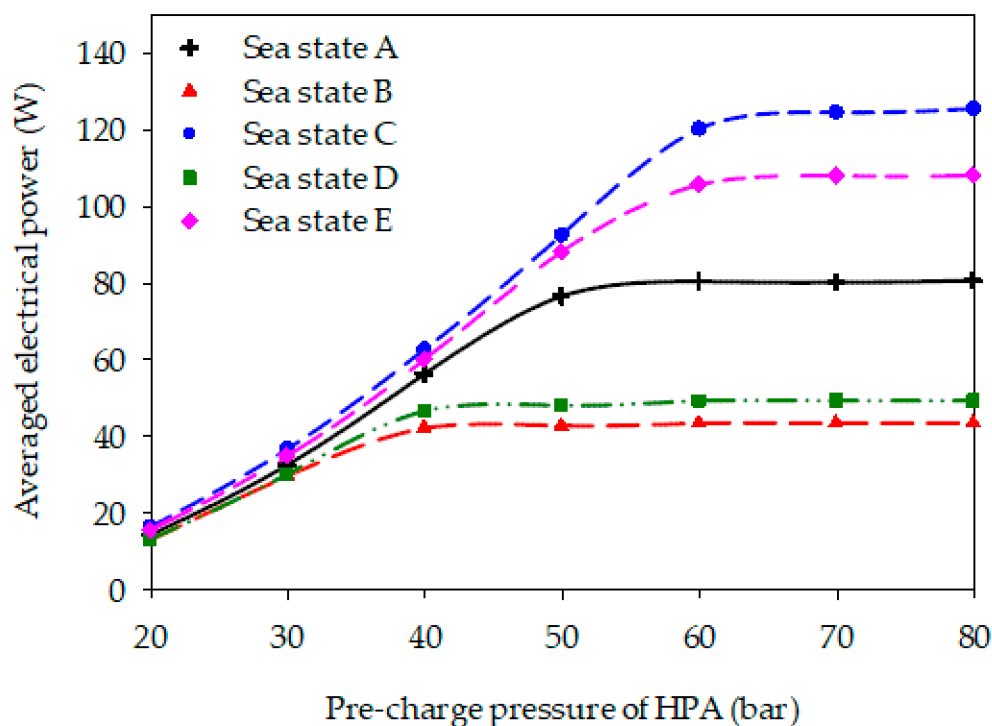

Figure 11. Averaged power of generator versus pre-charge pressure of HPA corresponding to different sea states.

4.3.5. Case 5: Displacement of Hydraulic Motor

The fluid displacement of the hydraulic motor (D_{HM}) is another important influencing parameter in the HPTO unit. Referring to Equation (14), D_{HM} directly affects the power and torque of the hydraulic motor. Therefore, it is necessary to explore the effect of the D_{HM} on the power of the hydraulic motor and generator. From the preliminary survey, the smallest size hydraulic motor currently available from the available hydraulic equipment for HPTO application 6 cc/rev. Thus, the variation range of D_{HM} was set within 6 to 20 cc/rev and the value of D_{HM} was incrementally varied by 2 cc/rev. Figure 12 illustrates the effect of D_{HM} on the averaged generated power from the generator corresponding to different sea states. From the figure, it is clearly shown that the averaged generated power increases with the increase in D_{HM} and then starts to decrease after reaching an optimal value of D_{HM} for all sea states. The figure shows that a higher value of D_{HM} can be implemented with a large significant wave height and peak period sea states. The result indicates that the value of D_{HM} can be considered up to 10 cc/rev for sea states C and E, but only up to 8 cc/rev for sea states B and D. This may be due to the high operating pressure of HPTO during the large significant wave height and peak period sea states. At the optimal value of D_{HM}, the average generated power for sea states A to E can reach up to 72 W, 44 W, 102 W, 50 W and 90 W, respectively. Apart from that, the result also shows that the overestimated value of D_{HM} was more affected in HPTO performance at the small significant wave height and peak period sea states. For example, the average generated power in sea states B and D was reduced by up to 59% and 60% once the value of D_{HM} was increased from the optimal (8 cc/rev) to 18 cc/rev; while for sea states C and E, the average generated power in sea states C and E were reduced by up to 46% and 47% once the value of D_{HM} was increased from the optimal (10 cc/rev) to 18 cc/rev. However, this was vice-versa

during the underestimated value of D_{HM}, in which the HPTO performance in the large wave height and period sea states was more affected by the D_{HM}. The figure clearly shows that the averaged generated power for sea states C and E were significantly reduced by 53% and 50%. Therefore, the result reveals that the underestimation and overestimation of the D_{HM} can significantly reduce the power generated from the generator.
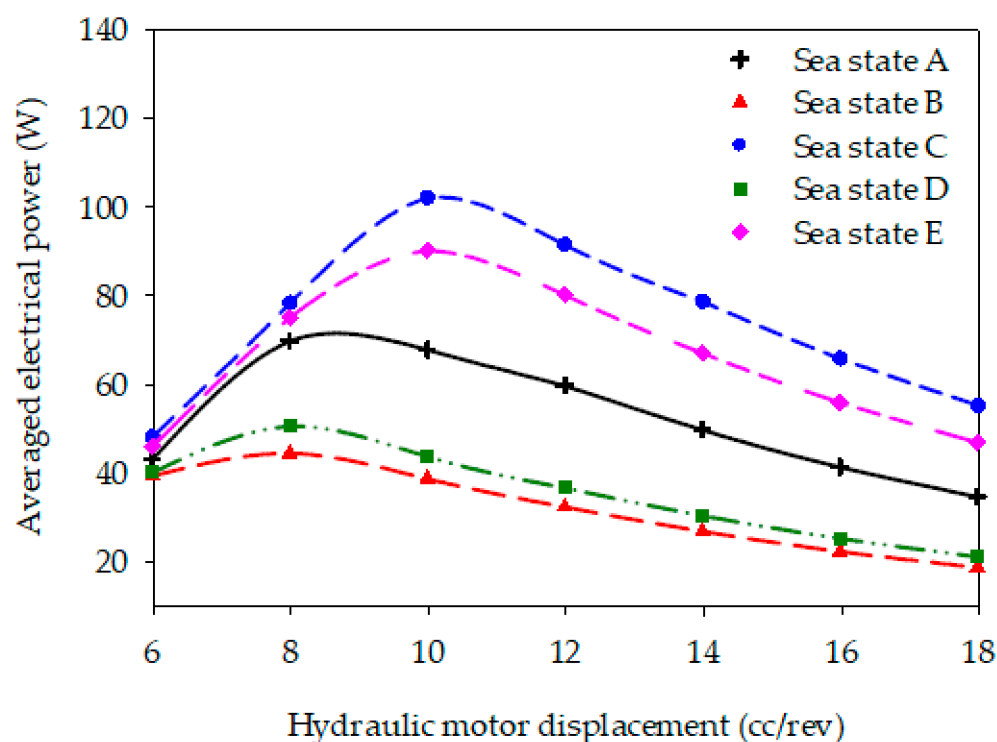

Figure 12. Averaged power of generator versus fluid displacement of HM corresponding to different sea states.

4.3.6. Case 6: Damping Coefficient of Electrical Generator

The damping coefficient (d_G) is different for each generator. As mentioned in [11], the d_G of each generator is subjected to its type, capacity, etc. Technically, generated output power is affected by the d_G. Since the generator is one of the major components of the HPTO unit, the effect of the d_G on the performance of the HPTO needs to be investigated. Thus, the effect of d_G on the generated power from the HPTO unit was investigated in this study. In this case, the d_G was varied from 0.1 to 1.2 Nm/(rad/s) with increments of 0.1 Nm/(rad/s) in each sequence. Figure 13 depicts the effect of d_G on the averaged generated power corresponding to five different sea states. From the figure, it can be seen that the optimal d_G that achieves the highest averaged power was sensitive to changes in significant wave height and peak wave period. During the nominal sea state, the optimal d_G was found to around 0.3 Nm/(rad/s), while, for the short and long peak wave period sea states (sea states B and C), the optimal d_G was found to be around 0.35 and 0.26 Nm/(rad/s). Meanwhile, for the small and large significant wave height sea states (sea states D and E), the optimal d_G was found at around 0.34 and 0.24 Nm/(rad/s), respectively. The result also indicates that the overestimation of d_G badly reduced the averaged generated power for all sea states, particularly sea states A, C and E. As can be seen in the figure, the average generated power for sea states A to E was reduced by 73%, 62%, 72%, 63% and 74% of its optimal value, respectively, due to overestimation of d_G by up to 1.3 Nm/(rad/s). Hence, from the results, it can be said that the generator damping coefficient needs to be optimally controlled to maximize power absorption from the ocean. Thus, the use of several damping control strategies, as suggested in [17], can be considered in the HPTO unit.
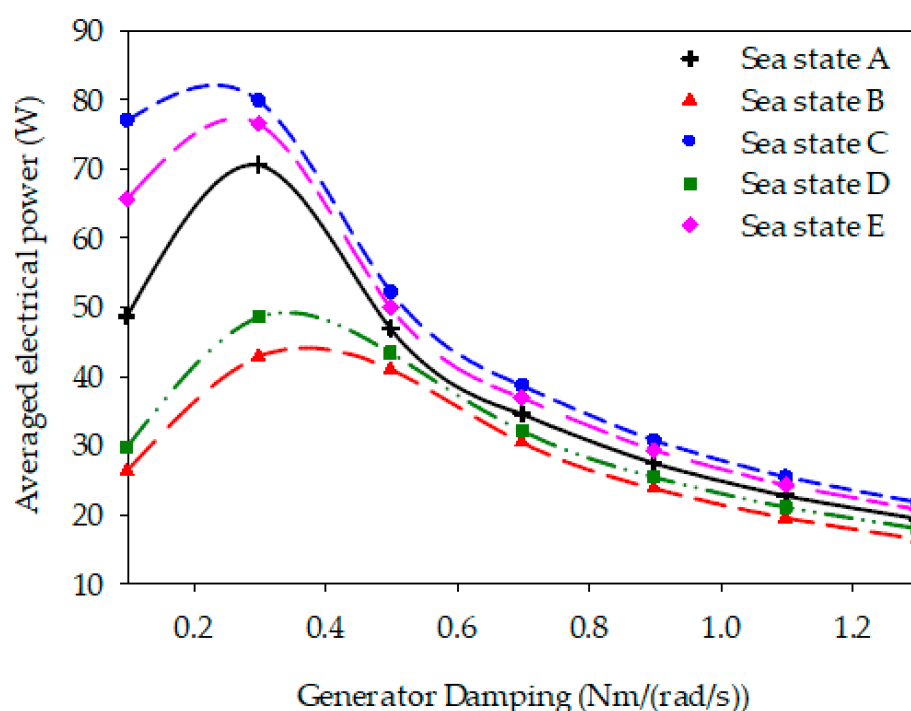
Figure 13. Averaged power of generator versus damping of generator corresponding to different sea states.

5. Conclusions

A comprehensive analysis of the effects of the important HPTO parameters on performance in generating usable electricity was conducted in the present study. Six critical parameters of the HPTO unit, including vertical mounting and the piston size of the HA, volume capacity and pre-charge pressure of HPA, displacement of HM and damping coefficient of the generator were considered. A simulation study was conducted using MATLAB/Simulink software, in which a complete model of WEC with the HPTO unit was developed using the Simscape fluids toolbox in MATLAB/Simulink. Five different irregular sea state inputs were used to evaluate the effect of each HPTO parameter against the different significant wave heights and peak periods. From the investigation, the following conclusion can be drawn:

(1) For case 1, the effect of the vertical mounting position (L_2) of the hydraulic actuator on the power generated by the generator was obtained. From the simulation result, it was found that the averaged power generated increased along with an increase of L_2 for all sea states and then decreased after reaching the optimal distance. At smaller L_2 (0.1 m), the averaged generated power for sea states A to E was reduced by 88%, 91%, 82%, 90% and 84% of their optimal values, respectively. The value of L_2 is sensitive to the significant wave height and peak wave period, in which the best of L_2 is larger during the large significant wave height and peak wave period sea state.

(2) For case 2, the averaged power generated was increased along with the increase of piston size (d_p) for all sea states. However, the average power was decreased for the over-sized of d_p state. The simulation result shows a d_p sensitive to the significant wave height and peak wave period. Thus, a large size of d_p should be used in the large significant wave height and peak wave period sea state.

(3) For case 3, the simulation results demonstrate that the volume capacity of HPA ($V_{HPA,cap}$) is less sensitive to changes in small significant wave height and peak wave period sea state, and inversely for a large significant wave height and peak wave period sea state, where the increase of $V_{HPA,cap}$ reduced the averaged power generated. This is due to more power accumulated in the HPA rather than directly flowing to

the hydraulic motor. Thus, an appropriate $V_{HPA,cap}$ should be selected based on the HPTO capacity to avoid this power reduction.

(4) For case 4, the simulation result shows that the pre-charge pressure of HPA ($P_{HPA,0}$) should be higher for the large significant wave height and peak wave period sea state rather than the small significant wave height and peak wave period sea state.

(5) For case 5, the investigation results reveal that the underestimated and overestimated hydraulic motor displacement (D_{HM}) was significantly sensitive to wave height and peak wave period. Thus, a variable displacement hydraulic motor with a robust control strategy should be considered.

(6) For case 6, the simulation results found that overestimated damping coefficient of the generator (d_G) hardly reduced the averaged generated power. Thus, d_G needs to be optimally controlled using appropriate damping control strategies to maximize power absorption from the ocean waves.

The present investigation studies may help researchers and engineers of WECs to improve the efficiency of their systems. The optimization of the critical parameters above is another attractive issue in terms of maximizing the generated power from the HPTO unit. Thus, it is suggested that further research regarding the HPTO parameter optimization using heuristic optimization algorithms should be conducted.

Author Contributions: M.A.J., conceptualization, methodology, software, data curation, analysis, writing—original draft; M.Z.I., writing—review and editing and supervision, project administration, funding acquisition; M.Z.D., conceptualization, methodology, writing—review and editing and supervision; Z.M.Y., software, data curation, analysis and writing—original draft; A.A. data curation, analysis and writing—review and editing. All authors have read and agreed to the published version of the manuscript.

Institutional Review Board Statement: Not applicable.

Informed Consent Statement: Not applicable.

Data Availability Statement: Data available on request due to restrictions of privacy.

Conflicts of Interest: The authors declare no conflict of interest.

References

1. Melikoglu, M. Current status and future of ocean energy sources: A global review. *Ocean Eng.* **2018**, *148*, 563–573. [CrossRef]
2. Farrok, O.; Ahmed, K.; Tahlil, A.D.; Farah, M.M.; Kiran, M.R.; Islam, M.R. Electrical power generation from the oceanic wave for sustainable advancement in renewable energy technologies. *Sustainability* **2020**, *12*, 2178. [CrossRef]
3. Ahamed, R.; McKee, K.; Howard, I. Advancements of wave energy converters based on power take off (PTO) systems: A review. *Ocean Eng.* **2020**, *204*, 107248. [CrossRef]
4. Al Shami, E.; Zhang, R.; Wang, X. Point absorber wave energy harvesters: A review of recent developments. *Energies* **2019**, *12*, 47. [CrossRef]
5. Falcão, A.F. Wave energy utilization: A review of the technologies. *Renew. Sustain. Energy Rev.* **2010**, *14*, 899–918. [CrossRef]
6. Yusop, Z.M.; Ibrahim, M.Z.; Jusoh, M.A.; Albani, A.; Rahman, S.J.A. Wave-Activated Body Energy Converter Technologies: A Review. *J. Adv. Res. Fluid Mech. Therm. Sci.* **2020**, *76*, 76–104. [CrossRef]
7. Sheng, W.; Lewis, A. Power takeoff optimization for maximizing energy conversion of wave-activated bodies. *IEEE J. Ocean. Eng.* **2016**, *41*, 529–540. [CrossRef]
8. Drew, B.; Plummer, A.R.; Sahinkaya, M.N. A review of wave energy converter technology. *Proc. Inst. Mech. Eng. Part A J. Power Energy* **2009**, *223*, 887–902. [CrossRef]
9. Titah-Benbouzid, H.; Benbouzid, M. An up-to-date technologies review and evaluation of wave energy converters. *Int. Rev. Electr. Eng.* **2015**, *10*, 52–61. [CrossRef]
10. Kukner, A.; Erselcan, İ.Ö. A review of power take-off systems employed in wave energy. *J. Nav. Sci. Eng.* **2014**, *10*, 32–44.
11. Jusoh, M.A.; Ibrahim, M.Z.; Daud, M.Z.; Albani, A.; Yusop, Z.M. Hydraulic power take-off concepts for wave energy conversion system: A review. *Energies* **2019**, *12*, 4510. [CrossRef]

12. He, X.; Xiao, G.; Hu, B.; Tan, L.; Tang, H.; He, S.; He, Z. The applications of energy regeneration and conversion technologies based on hydraulic transmission systems: A review. *Energy Convers. Manag.* **2020**, *205*, 112413. [CrossRef]

13. Hansen, R.H.; Kramer, M.M.; Vidal, E.; Hansen, R.H.; Kramer, M.M.; Vidal, E. Discrete displacement hydraulic power take-off system for the wavestar wave energy converter. *Energies* **2013**, *6*, 4001–4044. [CrossRef]

14. Liu, C.; Yang, Q.; Bao, G. Influence of hydraulic power take-off unit parameters on power capture ability of a two-raft-type wave energy converter. *Ocean Eng.* **2018**, *150*, 69–80. [CrossRef]

15. Zou, S.; Abdelkhalik, O. Control of Wave Energy Converters with Discrete Displacement Hydraulic Power Take-Off Units. *J. Mar. Sci. Eng.* **2018**, *6*, 31. [CrossRef]

16. Ding, B.; Cazzolato, B.S.; Arjomandi, M.; Hardy, P.; Mills, B. Sea-state based maximum power point tracking damping control of a fully submerged oscillating buoy. *Ocean Eng.* **2016**, *126*, 299–312. [CrossRef]

17. Jianan, X.; Tao, X. MPPT Control of Hydraulic Power Take-Off for Wave Energy Converter on Artificial Breakwater. *J. Mar. Sci. Eng.* **2019**, *8*, 304. [CrossRef]

18. Liu, C.; Yang, Q.; Bao, G. Performance investigation of a two-raft-type wave energy converter with hydraulic power take-off unit. *Appl. Ocean Res.* **2017**, *62*, 139–155. [CrossRef]

19. Xuhui, Y.; Qijuan, C.; Zenghui, W.; Dazhou, G.; Donglin, Y.; Wen, J.; Weiyu, W. A novel nonlinear state space model for the hydraulic power take-off of a wave energy converter. *Energy* **2019**, *180*, 465–479. [CrossRef]

20. Jusoh, M.A.; Ibrahim, M.Z.; Daud, M.Z.; Yusop, Z.M.; Albani, A. An Estimation of Hydraulic Power Take-off Unit Parameters for Wave Energy Converter Device Using Non-Evolutionary NLPQL and Evolutionary GA Approaches. *Energies* **2020**, *14*, 79. [CrossRef]

21. Jusoh, M.A.; Ibrahim, M.Z.; Daud, M.Z.; Yusop, Z.M.; Albani, A.; Rahman, S.J.; Mohad, S. Parameters estimation of hydraulic power take-off system for wave energy conversion system using genetic algorithm. In *Proceedings of the IOP Conference Series: Earth and Environmental Science*; Institute of Physics Publishing: Bristol, UK, 2020; Volume 463, p. 12129.

22. Hansen, A.H.; Asmussen, M.F.; Bech, M.M. Model predictive control of a wave energy converter with discrete fluid power power take-off system. *Energies* **2018**, *11*, 635. [CrossRef]

23. Gaspar, J.F.; Calvário, M.; Kamarlouei, M.; Soares, C.G. Design tradeoffs of an oil-hydraulic power take-off for wave energy converters. *Renew. Energy* **2018**, *129*, 245–259. [CrossRef]

24. Gaspar, J.F.; Calvário, M.; Kamarlouei, M.; Guedes Soares, C. Power take-off concept for wave energy converters based on oil-hydraulic transformer units. *Renew. Energy* **2016**, *86*, 1232–1246. [CrossRef]

25. Penalba, M.; Sell, N.P.; Hillis, A.J.; Ringwood, J.V.; Penalba, M.; Sell, N.P.; Hillis, A.J.; Ringwood, J.V. Validating a wave-to-wire model for a wave energy converter—Part I: The hydraulic transmission system. *Energies* **2017**, *10*, 977. [CrossRef]

26. Shadman, M.; Estefen, S.F.; Rodriguez, C.A.; Nogueira, I.C.M. A geometrical optimization method applied to a heaving point absorber wave energy converter. *Renew. Energy* **2018**, *115*, 533–546. [CrossRef]

27. Coiro, D.P.; Troise, G.; Calise, G.; Bizzarrini, N. Wave energy conversion through a point pivoted absorber: Numerical and experimental tests on a scaled model. *Renew. Energy* **2016**, *87*, 317–325. [CrossRef]

28. Chen, Z.; Zhou, B.; Zhang, L.; Sun, L.; Zhang, X. Performance evaluation of a dual resonance wave-energy convertor in irregular waves. *Appl. Ocean Res.* **2018**, *77*, 78–88. [CrossRef]

29. Sun, P.; Li, Q.; He, H.; Chen, H.; Zhang, J.; Li, H.; Liu, D. Design and optimization investigation on hydraulic transmission and energy storage system for a floating-array-buoys wave energy converter. *Energy Convers. Manag.* **2021**, *235*, 113998. [CrossRef]

30. Liu, Z.; Qu, N.; Han, Z.; Zhang, J.; Zhang, S.; Li, M.; Shi, H. Study on energy conversion and storage system for a prototype buoys-array wave energy converter. *Energy Sustain. Dev.* **2016**, *34*, 100–110. [CrossRef]

31. Liang, C.; Ai, J.; Zuo, L. Design, fabrication, simulation and testing of an ocean wave energy converter with mechanical motion rectifier. *Ocean Eng.* **2017**, *136*, 190–200. [CrossRef]

32. Zurkinden, A.S.; Ferri, F.; Beatty, S.; Kofoed, J.P.; Kramer, M.M. Non-linear numerical modeling and experimental testing of a point absorber wave energy converter. *Ocean Eng.* **2014**, *78*, 11–21. [CrossRef]

33. Rahmati, M.T.; Aggidis, G.A. Numerical and experimental analysis of the power output of a point absorber wave energy converter in irregular waves. *Ocean Eng.* **2016**, *111*, 483–492. [CrossRef]

34. Jama, M.A.; Noura, H.; Wahyudie, A.; Assi, A. Enhancing the performance of heaving wave energy converters using model-free control approach. *Renew. Energy* **2015**, *83*, 931–941. [CrossRef]

35. Forehand, D.I.M.; Kiprakis, A.E.; Nambiar, A.J.; Wallace, A.R. A Fully Coupled Wave-to-Wire Model of an Array of Wave Energy Converters. *IEEE Trans. Sustain. Energy* **2016**, *7*, 118–128. [CrossRef]

36. Windt, C.; Davidson, J.; Ringwood, J.V. High-fidelity numerical modelling of ocean wave energy systems: A review of computational fluid dynamics-based numerical wave tanks. *Renew. Sustain. Energy Rev.* **2018**, *93*, 610–630. [CrossRef]